Cell Host & Microbe, Volume *13*

Supplemental Information

The Herpesvirus VP1/2 Protein Is an Effector of Dynein-Mediated Capsid Transport and Neuroinvasion

Sofia V. Zaichick, Kevin P. Bohannon, Ami Hughes, Patricia J. Sollars, Gary E. Pickard, and Gregory A. Smith

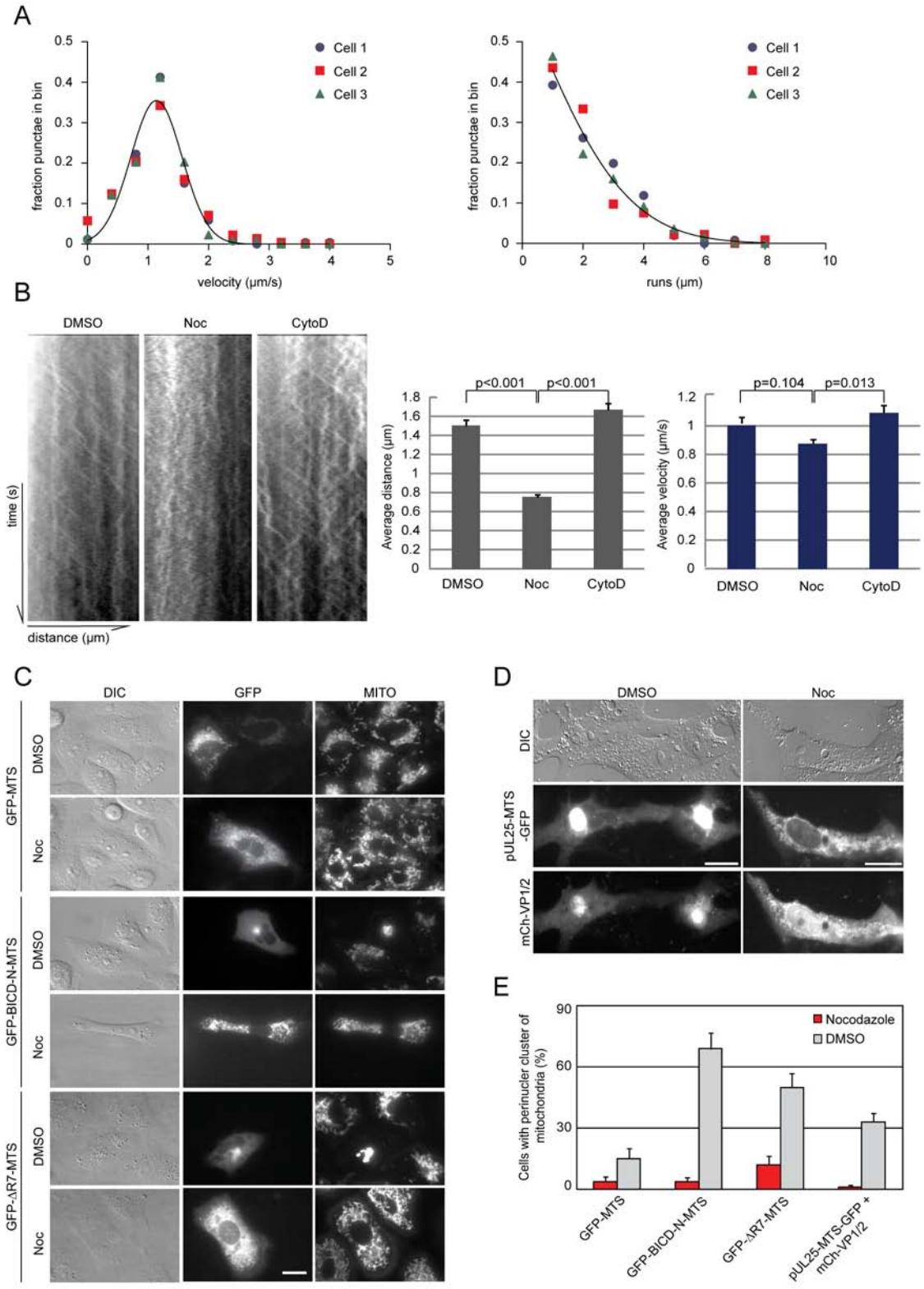

Figure S1, related to Figure 2. Analysis of GFP-VP1/2ΔR7 motion in transiently transfected Vero cells and microtubule dependence of VP1/2-induced redistribution of mitochondria. (A) Run lengths of continuous motion and corresponding velocities.

Recordings were captured at 50 frames/s (300 frames total). More than 200 GFP punctae that moved > 0.5 μm were traced per cell. Runs of continuous motion were grouped in 0.4 μm bins and corresponding velocities were grouped in 1 μm/s bins. Non-linear regression was used to fit a Gaussian distribution to velocities from all cells (R^2>0.95). Run lengths were fit by exponential decay (R^2>0.95). (B) VP1/2 movement requires microtubules, but not filamentous actin. Recordings were captured at 10 frames/s (300 frames total). Representative examples of kymographs from cells treated with vehicle control (DMSO), 10 μM nocodazole (Noc) or 0.5 μM cytochalasin D (CytoD) for 1 h before imaging are shown. Average run lengths and velocities are plotted on the right ± the standard error of mean (SEM). P-values were determined by one-way analysis of variance (ANOVA) with a post-hoc Tukey test.
All recordings were captured 16-20 hpt from cells exhibiting numerous distinct diffraction-limited fluorescent punctae. Three cells (3 kymographs from each cell) were analyzed in each experiment. Kymographs were generated using the “Multi-line” tool with a width of 7 pixels without subtraction. Run lengths and velocities were measured from kymographs along 15 μm paths for panel A or 20 μm for panel B.
(C) Vero cells transiently expressing indicated constructs were treated with vehicle control (DMSO) or 10 μM nocodazole (Noc) for 3 h before imaging and stained with MitoTracker Red for 30 min before imaging. (D) Vero cells were co-transfected with indicated constructs and treated as described above. (E) Proportions of cells exhibiting mitochondria redistribution to the perinuclear region ± SEP (standard error of the proportion). Cells were imaged 18-24 hpt.

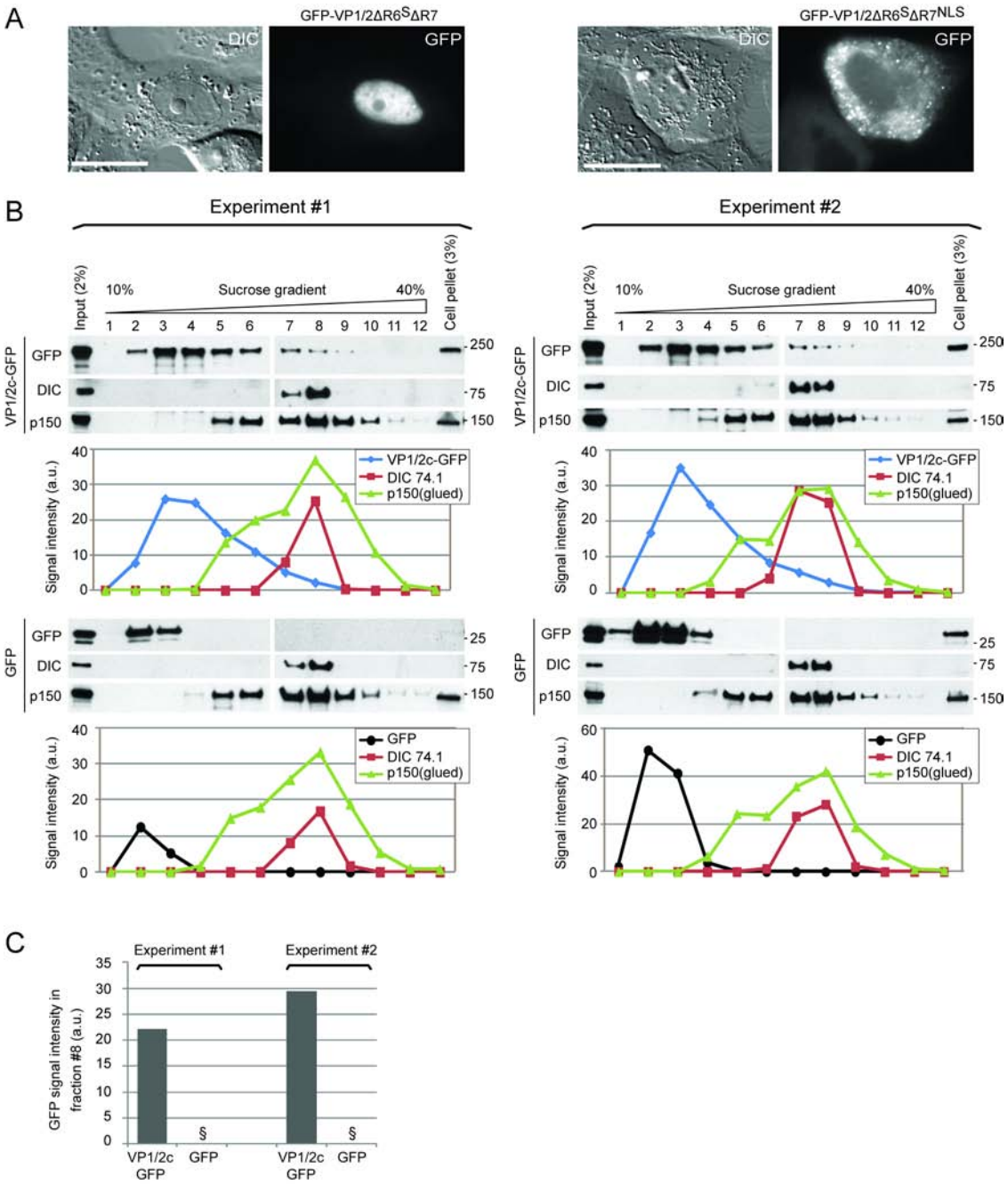

Figure S2, related to Figure 3. Control for NLS activity in truncated VP1/2ΔR6^{S}ΔR7, and co-sedimentation of truncated VP1/2c with the 20S dynein/dynactin complex. (A) Removal of region 6 resulted in VP1/2 localization to the nucleus by unmasking a cryptic nuclear localization signal (NLS) in region 2 of the protein, as previously described for HSV-1 VP1/2 (Abaitua and O'Hare, 2008). Because GFP-VP1/2ΔR6ΔR7 and GFP-VP1/2ΔR6^{S}ΔR7 displayed nuclear restricted fluorescence that may have accounted for the poor interaction with dynactin, versions of each truncation carrying a K^{285}RRR>AAAA NLS mutation was produced and confirmed to localize in the cytoplasm

of transfected Vero cells. Further analysis of these constructs is included in Figure 3E. Images were captured approximately 18 hpt. Scale bar, 20 µm.
(B) The VP1/2 fragment consisting of regions 6 and region 7 (VP1/2c-GFP) or GFP alone (GFP) were transiently expressed in HEK293 cells. Cleared cell lysates were sedimented through gradients of 10-40% sucrose and collected in twelve fractions. Following gel electrophoresis, samples were immunoblotted for GFP, DIC 74.1 (dynein component), and p150/glued (dynactin component). Results from two independent experiments are shown. Densitometry was analyzed in ImageJ and illustrated in line graphs below each blot. Crude cell lysate (Input) and pellets obtained after clearing the cell lysates were included for comparison, with the percentages indicating amount of each loaded on the gel. (C) GFP signal intensity in the peak dynein fraction (fraction #8). The GFP control had no signal in fraction #8 (§).

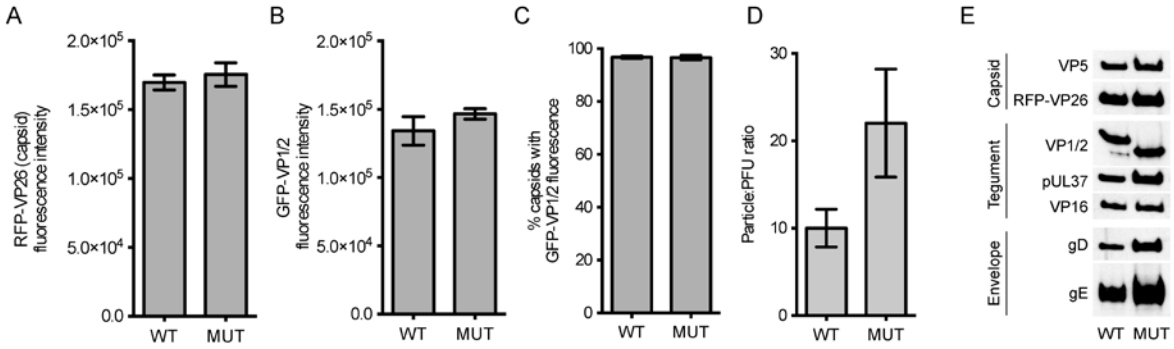

Figure S3, related to Figure 4. Incorporation of structural proteins into WT and MUT viruses. (A-C) Incorporation of GFP-VP1/2 into WT and MUT viruses by single particle analysis. Three independent isolations of extracellular, dual-fluorescent PRV particles (mRFP1-VP26 + GFP-VP1/2) were pelleted out of solution and spotted on coverslips for imaging by widefield fluorescence microscopy. Between 350 and 2000 capsid-containing particles from each isolation were imaged. (A) Average red fluorescence intensity of individual virus particles. (B) Average green fluorescence intensity of particles analyzed in panel A. (C) Percentage of red-fluorescent capsids that colocalized with GFP-VP1/2. (D) Extracellular capsid-containing fluorescent viral particles were counted and compared to the number of plaque forming units (PFU) as determined by plaque assay. Error bars represent SEM. The approximate 2-fold difference between WT and MUT was not significant as determined by Student's t-test. (E) Incorporation of VP1/2, pUL37, VP16, gD and gE into WT and MUT PRV virions. 1.75 x 10^7 PFU of purified extracellular H-particles were separated by gel electrophoresis and probed for the indicated capsid, tegument, and envelope proteins.

Table S1. Description of recombinant PRV used in this study, related to Experimental Procedures

PRV-GS#	Fluorescent tag	VP1/2 allele	Aliases	Experiment
847	RFP-pUL35	WT	WT	virus propagation neurovirulence retrograde kinetics virion composition
2111	RFP-pUL35	$\Delta R6^S$	MUT	
4079	RFP-pUL35	WT	REP	
4379	pUL25/GFP	WT	GFP-WT	nuclear rim delivery
4284	pUL25/mCherry	WT	RFP-WT	
4444	pUL25/GFP	$\Delta R6^S$	GFP-MUT	
4482	pUL25/mCherry	$\Delta R6^S$	RFP-MUT	
909	RFP-pUL35	GFP-WT	WT	virion composition
2175	RFP-pUL35	GFP-$\Delta R6^S$	MUT	

Table S2. Primers used to introduce in-frame deletions and codon changes in the VP1/2 gene (UL36) of the pBecker3 infectious clone by two-step RED-mediated recombination, related to Experimental Procedures

Final BAC	Primers [(a)]	BAC target	Codon changes in UL36
pGS3342	5'- AAAGATTTTTCCCCCACGCGCGTGTGTTATTTCAGCCATG*GTGAGCAAG GGCGAGGAG* 5'-GCGGCAGGGCCATCGGGTGCACGGAGGGCGCGTCGGCCGT*CTTGTACA GCTCGTCCATGC*	pGS847	Δ6-225 (ΔR1)
pGS3047	5'-GGCGAGACGTACCTCGTGGACGAGCCGTACGTGGAGCGGGCGGTGGCG AGCCAGGAGGAC*AGGATGACGACGATAAGTAGGG* 5'-GCCGCCCGCCGACCGTGTGCGTGCTGCTCAGGTCCTCCTGGCTCGCCAC CGCCCGCTCCAC*CAACCAATTAACCAATTCTGATTAG*	pGS909	Δ226-292 (ΔR2)
pGS3064	5'- CAGAAGCGGCCGAGCATGCCCAAGCGGCGCCGGCCCCCGTGGCCGGC GCCGTGCGCCGTC*AGGATGACGACGATAAGTAGGG* 5'-CGCGCCCAGGATGGGCTCGAAGAGCGCGGCGACGGCGCACGGCGCCG GCCACGGGGGCCG*CAACCAATTAACCAATTCTGATTAG*	pGS909	Δ300-396 (ΔR3)
pGS2808	5'-CTGCAGGACTTTCTGGTGGAGAACGGCGCCCGCACCCACGGGGAGCGC GACCGCGACGGG*AGGATGACGACGATAAGTAGGG* 5'-AGGTTCTTGAGGTTGGCCAGCTCGAGGGCCCCGTCGCGGTCGCGCTCCC CGTGGGTGCG*CAACCAATTAACCAATTCTGATTAG*	pGS909	Δ391-1287 (ΔR4)
pGS2810	5'-GCGCCACGCGCCTGCTGCGCGAGGTGGTGGACGCGGCGGCGGCGCCGC CCGAGCCGCCG*AGGATGACGACGATAAGTAGGG* 5'-TCGTCCTCGAGCGTGAAGCCCGGGCGTCGCGGCGGCTCGGGCGGCGCC GCCGCCGCGTC*CAACCAATTAACCAATTCTGATTAG*	pGS909	Δ1288-2019 (ΔR5)
1) pGS2111 2) pGS4400	5'-GGCGACGCCCGCGTGGACCCGGCCACCTCGGAGGAGCTGTACGGCGCC GCACCACCGCCG*AGGATGACGACGATAAGTAGGG* 5'-CGTCGGGGCCGGCCGCGAAGGTGGTGGGGCCGGCGGTGGTGCGGCGCC GTACAGCTCCTC*CAACCAATTAACCAATTCTGATTAG*	1) pGS847 2) pBecker3	Δ2080-2796 ($\Delta R6^S$)
pGS2955	5'- ACCGCTCCCGCCGCCGCCGCGGGTCCAGAAGCGGCCGAGCATG**CCAG CTGCCGCG**GCGCCCCCGTGGCCGGCG*AGGATGACGACGATAAGTAGGG* 5'-CGTGTGCGTGCTGCTCAGGTCCTCCTGGCTCGCCGGCCACGGGGGCG C**CGCGGCAGCTGG**CATGCTCGGCCGC*CAACCAATTAACCAATTCTGATTAG*	pGS909	K^{285}RRRR>AAAA
pGS3294	5'- ACCGCTCCCGCCGCCGCCGCGGGTCCAGAAGCGGCCGAGCATG**CCAG CTGCCGCG**GCGCCCCCGTGGCCGGCG*AGGATGACGACGATAAGTAGGG* 5'-CGTGTGCGTGCTGCTCAGGTCCTCCTGGCTCGCCGGCCACGGGGGCGC **CGCGGCAGCTGG**CATGCTCGGCCGC*CAACCAATTAACCAATTCTGATTAG*	pGS2175	Δ2080-2796 ($\Delta R6^S$) + K^{285}RRRR>AAAA

[(a)] Italicized nucleotides share homology to the pEP-GFP-in template (pGS3342) or the pEPkan-S2 template (all others); bold nucleotides indicate codon changes

Table S3. VP1/2 expression plasmids used in this study, related to Experimental Procedures

Expression plasmid	BAC source	pGS1292 subclone	Insert
pGS3384	pGS909	pGS2545	GFP-(R1-R6)
pGS3364	pGS3342	pGS3359	GFP-(R2-R6)
pGS3226	pGS3047	pGS3062	GFP-(R1-R6) ΔR2
pGS3227	pGS3064	pGS3114	GFP-(R1-R6) ΔR3
pGS3241	pGS2808	pGS2832	GFP-(R1-R6) ΔR4
pGS3242	pGS2810	pGS2833	GFP-(R1-R6) ΔR5
pGS3229	pGS2175	pGS2597po	GFP-(R1-R6) $\Delta R6^{S}$
pGS3157	pGS2955	pGS3014	GFP-$(R1\text{-}R6)^{NLS}$
pGS3322	pGS3294	pGS3306	GFP-$(R1\text{-}R6)^{NLS}\Delta R6^{S}$
pGS3296	pGS2955	pGS3288	GFP-$(R1\text{-}R5)^{NLS}$
pGS3337	pGS1903	pGS3335	(R5-R7)-GFP
pGS3476	pGS2176	pGS3470	(R5-R7) $\Delta R6^{S}$-GFP
pGS4351	pGS909	pGS4350	GFP-(R1-R7)
pGS1907	pGS909	pGS1514	mCherry-(R1-R7)
pGS4269	pGS1903	pGS4257	(R1-R7)-GFP
pGS4274	pGS2176	pGS2279	(R1-R7) $\Delta R6^{S}$-GFP

Supplemental Experimental Procedures

Cells and virus propagation. Vero (African green monkey kidney epithelial), HEK 293 (human embryonic kidney) and PK15 (pig kidney epithelial) cells were grown in DMEM (Dulbecco's Modified Eagle Medium, Invitrogen) supplemented with 10% BGS (bovine growth supplement, HyClone). BGS levels were reduced to 2% during infection. Primary dorsal root ganglia (DRG) from embryonic chicken (E8-E9) were cultured for 2 days on polyornithine and laminin treated coverslips as previously described (Smith, 1998; Smith et al., 2001).

Infectious clones of PRV-Becker were transfected into PK15 cells as previously described (Luxton et al., 2005). The resultant stock of virus was passaged once more to create a working stock. Titers of working stocks were obtained by performing plaque assays on PK15 or Vero cells as previously described (Smith and Enquist, 1999).

Viruses. All viruses used in this study were derived from the pBecker3 infectious clone and are listed in Table S1 (Smith et al., 2000). Viruses encoding fluorescent capsid tags were previously described: PRV-GS847 (Smith et al., 2004), PRV-GS4379, and PRV-GS4284 (Bohannon et al., 2012). PRV-GS847 encodes a mRFP1-VP26 fusion, whereas PRV-GS4379 and PRV-GS4284 encode UL25 with a double in-frame GFP or mCherry insertion, respectively. PRV-GS909 encodes mRFP1-VP26 and GFP-VP1/2 fusions, and was previously described (Luxton et al., 2005).

The UL36 $R6^S$ deletion (codons 2080-2796 of 3095 total) was introduced by two-step red-mediated recombination (Tischer et al., 2006) using primers indicated in Table S2. Codon numbering was based on the PRV-Becker sequence; GenBank JF797219.1 (Szpara et al., 2011). This resulted in pGS2111 (derived from pGS847) and pGS4400 (derived from pBecker3). The pGS2111 clone was further modified to encode GFP fused to the amino terminus of VP1/2, using primers: 5' AAAGATTTTTCCCCCACGCGCGTGTGTTATTTCAGCCATGGTGAGCAAGGGCGAG and 5' CATACTGATTACGATAGCCGACGACCACCGCGTCGGCCGTCTTGTACAGCTCGTC. The regions of homology with pEP-EGFP-in template are underlined. This resulted in pGS2175. The pGS4400 clone was further modified to encode a fluorescent capsid tag by inserting GFP or mCherry into UL25 as previously described (Bohannon et al., 2012). This resulted in pGS4444 and pGS4482, respectively.

To repair the UL36 $R6^S$ deletion in pGS2111, three sequential recombination reactions were performed. First, an I-SceI endonuclease site and kanamycin cassette (I-sceI/kan) was inserted into the $R6^S$ region of UL36 using the following primers: 5' GGGCTCGGAGTCCGATGTCCCCGGAGGAGAGCGGGTCCGATGCTGGTCTGGTCCGACCGTCAACCAATTAACCAATTCTGATTAG and 5' AAAGCGGGGCGCGCAGACAAGTGCGAACACACGGTCGGACCAGACCAGCATCGGACCCGCAGGATGACGACGATAAGTAGGG. The regions of homology with pEPkan-S2 template are underlined. This resulted in pGS3909. Second, the I-sceI/kan cassette with UL36 flanking sequences that span beyond the $R6^S$ deletion were recombined into a small R6K plasmid, pGS1292, as previously described (Coller et al., 2007). A linear fragment of pGS1292 was amplified using the primers 5'GAGCGTGAAGCCCGGGCGTCGCGGCGGCTCGGGCGGCGCCATAAGCTTGTCATCCATATCACCACG (the HindIII restriction site is underlined) and 5'CTGGTGGACTCGCAGCTGGCGGTGTCGCGCGTGCTCTGGGATTTTTATC**GAATTC**CCACAT

GTGGAATTCCCAT (the BsaBI site is underlined and EcoRI site is bold). The resulting PCR product was inserted into UL36 upstream of region 6 based on homologies in the 5' end of each primer, and the pGS1292 sequence and downstream UL36 fragment containing the I-sceI/kan insertion was liberated by BsaBI digestion and self-ligation between two BsaBI sites: one engineered in the primer and the other an endogenous site downstream of the UL36 ORF. The circularized plasmid was cloned into S17-1 λpir *E. coli*, resulting in pGS4005. Third, the UL36/I-sceI/kan fragment was isolated from pGS4005 by EcoRI and HindIII digestion and recombined into pGS2111 and the I-sceI/kan cassette was removed by two-step red-mediated recombination. The resulting recombinant was confirmed to encode a WT UL36 allele by sequencing, and saved as pGS4079. Transfection of pGS2111, pGS2175, pGS4079, pGS4444, pGS4482 into PK15 cells resulted in PRV-GS2111, PRV-GS2175, PRV-GS4079, PRV-GS4444 and PRV-GS4482, respectively.

Plasmids. Several VP1/2 expression plasmids were made as GFP fusions. All were derived from pBecker3 BACs that were modified to encode GFP fused in-frame to either the amino (pGS909) or carboxyl terminus of VP1/2 (pGS1903) (Leelawong et al., 2012; Luxton et al., 2005). In addition, the VP1/2 ORF (UL36) was modified to encode in-frame deletions or a NLS mutation (KRRRR>AAAA) by two-step red-mediated recombination (Table S2). The UL36 alleles were subcloned from each BAC using a modified RED-GAM protocol as described previously (Coller et al., 2007). Briefly, a plasmid encoding a conditional R6K origin of replication and beta-lactamase (ampicillin resistance), pGS1292, was PCR amplified with primers that contained 5' homologies for targeted insertion into the pBecker3 derivatives into UL36. For BACs encoding GFP at the 5' end of UL36, pGS1292 was inserted at the 3' end of the desired region to be subcloned. For BACs encoding GFP at the 3' end of UL36, pGS1292 was inserted at the 5' end of the desired region to be subcloned. In either case, a BsrGI restriction site was included at the pGS1292 insertion. Using a corresponding BsrGI site within the GFP coding sequence, the UL36 fragment with the adjacent pGS1292 vector sequence was liberated by digestions with BsrGI and self ligated. The circularized plasmid was then cloned into S17-1 λpir *E. coli*, which allowed replication via the R6K origin. Finally, the cloned UL36 fragment was subcloned from the pGS1292 vector into either pEGFP-C1 or pEGFP-N1 (Clontech) to reconstitute the GFP coding sequence and establish the final expression plasmid (Table S3). Three additional VP1/2 expression plasmids were previously described: GFP-[R1-R5] (pGS1766), [R6-R7]-GFP (pGS1952), and GFP-[R1-R7] (pGS1521) (Lee et al., 2006; Leelawong et al., 2012).

A pUL25-GFP expression construct (pGS2099) was made using the same strategy as described above for the VP1/2 expression plasmids. The pBecker3 BAC was first modified by inserting the GFP coding sequence as an in-frame fusion to the 3' end of UL25, resulting in pGS1948. This was accomplished by two-step red-mediated recombination with primers: 5' TTTCTCTGCCTGGGCTATATCCCGCAGTTCGCCGCCGCCGTGAGCAAGGGCGAG and 5' CATGGCGGCGGCGGCGCGCGCGCGGAGACTGCGGGCTCACTTGTACAGCTCGTC (pEP-GFP-in homology regions are underlined). The pGS1292 vector with a flanking BsrGI site was subsequently inserted immediately 5' of the UL25 ORF, and the pGS1292/UL25-GFP sequence was cloned by BsrGI digestion and self ligation, resulting in pGS2097. Finally, the cloned UL25 ORF was subcloned from pGS2097 into pEGFP-N1 (Clontech) to reconstitute the GFP coding sequence and establish the final expression plasmid: pGS2099.

GFP-MTS and GFP-BICD-N-MTS expression plasmids were a kind gift of Dr. Akhmanova (Hoogenraad et al., 2003). MTS is a **m**embrane-**t**argeting **s**equence of the C-terminus (last 26 codons) of the ActA protein of *Listeria monocytogenes* that is efficient at targeting proteins to the outer mitochondrial membrane (Bear et al., 2000; Bubeck et al., 1997). GFP-BICD-N-MTS encodes the N-terminus (a.a. 1-594, out of 820) of Bicaudal D (BICD2) fused to GFP and MTS tags. To create fluorescent MTS-tagged PRV proteins, the MTS sequence was included in a primer sequence: 5'GGGGGATCC***TTA*****ATTATTTTTTCTTAATTGAATAATTTTGATAAACGCCCCTAAAGAGA ACACGCCAATAGCTAACATTGCAAGAATTAA**GAATTCTTTGGACACGGCGTCGACCTCGG CCAGG (BamHI and EcoRI sites are underlined, MTS sequence is in bold, stop codon is *italicized*) and 5' GGGAAGCTTCGGAGGCGCTCGTGCGCGCGCTCGAGG (the HindIII site is underlined). The 3' end of each primer provided homology to the UL37 ORF. The resulting PCR product was subcloned by EcoR1 and HindIII double digestion into pEGFP-C1. The resulting expression plasmid, pGS1823, encodes a GFP-pUL37-MTS fusion. The UL36-MTS expression construct was made by replacing the UL37 sequence in pGS1823 with UL36 [R1-R6] using BsrGI and EcoRI combined digestion, resulting in pGS2636. To fuse UL25-GFP with the MTS tag, UL25-GFP was first subcloned from pGS2099 into pEGFP-C2 (Clontech) using BsrG1 and SnaBI combined digestion, followed by subcloning into pGS1823 using AseI and EcoRI. The resulting pUL25-GFP-MTS fusion expression plasmid was saved as pGS2500.

Viral propagation and cell-cell spread kinetics. Cell-associated virus and supernatants for single-step growth curves were harvested from PK15 cells at 2, 5, 8, 12, and 24 hours post removal of inoculum and processed as previously described (Tirabassi and Enquist, 1998). Titers of all time-points were quantified by plaque assay on Vero cells and plotted with GraphPad Prism 4.

Plaque sizes of mRFP1-VP26 encoding viruses were measured by live-cell fluorescence imaging. Vero cells in 6-well trays were infected at a concentration of 100-300 plaque forming units (PFU) per well. Cells were overlaid with 3 ml methocel media (DMEM supplemented with 2% BGS and 10 mg/ml methyl cellulose) and plaques were allowed to expand for two to three days. Images of at least 30 isolated plaques from each virus strain were acquired with a Nikon Eclipse TE2000-U inverted microscope with a 0.30 NA 10 X objective and RFP filter set. To determine the plaque diameter, the average of two orthogonal diameter measurements were calculated for each plaque using ImageJ software v. 1.42q (Abramoff et al., 2004). Plaque diameters were expressed as a percentage of the diameter of PRV-GS847 which was always tested in parallel. There was no detectable difference in plaque diameters as a percentage of control plaque diameters between two and three days post infection. Values reported are an average of three independent experiments.

Virus retrograde transport kinetics. Analysis of viral particle movement was described previously (Bohannon et al., 2012). Briefly, two-day old DRG explants were infected with 7.0×10^6 PFU/coverslip of either WT, MUT or REP virus. Moving particles were detected by time-lapse fluorescence microscopy in the red fluorescence channel at 10 frames per second (100 ms exposures) during 30 second intervals. Particle velocities were determined using the kymograph function of the MetaMorph software package. Kymographs were generated using the "Multi-line" tool with a width of 20 pixels and "average background" subtraction. Entire particle paths, whether moving, stalled, or reversing, were traced within the kymograph using the "Multi-line" tool. Data was filtered post analysis to only include velocities of runs ≥ 0.5 µm. Histograms were made in GraphPad Prism 4, with bin sizes of 1 µm for run lengths and

0.4 μm/s for velocities. Built-in nonlinear regression analysis was used to fit Gaussian (velocity) or decaying exponential (run lengths) curves to the data. Three replicate experiments (n > 80 particles per experiment) were analyzed. P-values were determined by one-way analysis of variance and a post-hoc Tukey test.

To determine the efficiency of virus delivery to the nuclear rim, two-day old DRG explants were co-infected with two viruses at equal PFU (0.9-7.5 x 10^8 PFU/coverslip) in the following combinations: PRV-GS4379 (GFP-WT) and PRV-GS4284 (RFP-WT); PRV-GS4379 (GFP-WT) and PRV-GS4482 (RFP-MUT); or PRV-GS4284 (RFP-WT) and PRV-GS4444 (GFP-MUT). Because the accuracy of the assay readout required strict adherence of equal multiplicity for the reporter virus pairs, the viral stocks were titered both before and after infection of the explants. Neurons were infected with viral stocks that had previously been titered. The stocks were thawed, sonicated, and centrifuged at 300 x g for 5 min at RT to eliminate cell debris. A mixed stock of the two viruses containing equivalent titers for each virus was prepared and used to infect the DRG. In addition to being used to infect the neurons, the working dilutions of individual prepared viruses were used to confirm the titers of each virus. Neuron imaging experiments that were subsequently determined to have been infected with mixed stocks in which the two viruses differed in titer by more than two fold were discarded from the final analysis. Static images from multiple infected neurons were captured 2-3 h post infection with 100 ms RFP and 500 ms GFP sequential exposures. The three infection pairs were coded and analyzed blindly to determine the most predominant virus color present at specific nuclear rims. Results are presented as the averages of ≥ 5 experiments for each virus combination.

The frequency of capsid retrograde transport events (flux) was measured in distal axons of DRG. Two sets of three DRG explants were cultured for two days and infected at equal MOI (5.4-5.8 x 10^6 PFU/coverslip) with either RFP-WT (PRV-GS847) or RFP-MUT (PRV-GS2111). Each virus stock was thawed, sonicated, and centrifuged at 300 x g for 5 min at RT to eliminate cell debris before infection. Viral stocks were titered before and after the experiment as described above. Distal axons were imaged between 10 and 45 min post infection using 100 ms exposures for 10 s (132 μm x 132 μm frame). In total, 187 movies were recorded for RFP-MUT and 261 movies were recorded for RFP-WT. Particle entry flux was determined as the number of moving particles per recording. In order to be scored, particles had to travel at least 5 μm.

Virion composition. Analysis of GFP-VP1/2 incorporation into individual extracellular virions was previously described (Bohannon et al., 2012). Briefly, PK15 cells were infected with PRV-GS909 or PRV-GS2175 at an MOI of 5 and incubated for 18 h. Supernatants were cleared of cell debris by centrifugation at 4800 x g for 10 min. Cleared supernatant (8 ml) was underlaid with a 1 ml cushion of 10% Nycodenz in PBS in an SW41 centrifuge tube. Samples were centrifuged at 38500 x g for 60 min. Pelleted virus was resuspended in 0.1 ml PBS, and 65 μl of a 1:50 dilution in PBS was spotted onto a plasma-cleaned microscope slide and imaged on a Nikon Eclipse TE2000 U wide-field fluorescence microscope fitted to a Cascade II camera (Roper Scientific) and a 100×1.49 numerical aperture (NA) objective. GFP was imaged using a 470/40 nm excitation filter and 525/50 nm emission filter; mRFP1 and mCherry were both imaged using a 572/35 nm excitation filter and 632/60 nm emission filter. To determine particle brightness, multiple fields of particles were captured with exposure times of 1.5 s. A custom algorithm for the MetaMorph software package (Molecular Devices) was used to quantify fluorescence intensity of individual extracellular virus particles.

To determine particle:PFU ratio, PRV-GS909 and PRV-GS2175 were isolated as described above. The number of particles in the 0.1 ml PBS resuspension was determined by dilution such that individual capsid-positive fluorescent particles could be differentiated by widefield fluorescence microscopy (1:30 for PRV-GS909, 1:10 for PRV-GS2175). 2 µl of the diluted virus was spotted between a coverglass and slide. This created two very close, but differentiable planes (coverglass and slide). 25 fields were imaged for red capsid fluorescence; 5 in the center of the coverslip and 5 near each of the four corners. Both the top (slide) and bottom (coverglass) planes were imaged. Diffraction-limited red virions on the slide and coverglass were counted in each field. The total number of particles was extrapolated by multiplying the average number of particles per field by 78,872 (area of the coverslip/area of the image field), then multiplying by the dilution factor to determine particles/ml. PFU in the same samples were quantified by plaque assay on PK15 cells.

For Western blot analysis of viral protein incorporation into extracellular virions, PRV-GS847 and PRV-GS2111 H-particles were purified from infected cell supernatants by rate zonal ultracentrifugation in a 12–32% dextran gradient as described previously (Antinone and Smith, 2006; Leelawong et al., 2012). Samples were boiled for 5 minutes in final sample buffer, separated on a 4-20% precast Mini-PROTEAN TGX gel (Bio-Rad), and transferred to PVDF Immobilon-FL membrane (Millipore). Viral proteins were detected as follows: 1:1000 of mouse monoclonal anti-VP5 (3C10; a gift from Lynn Enquist), 1:5000 dilution of mouse monoclonal anti-gD (SC1, a gift from G. H. Cohen), 1:1000 dilution of rabbit polyclonal anti-gE (a gift from Lynn Enquist), 1:1000 dilution of chicken polyclonal anti-VP16 (VP16 1200; a gift from Lynn Enquist) and 1:1000 dilution of rabbit polyclonal anti-RFP (GenScript). To detect VP1/2 antigen, a rabbit polyclonal antibody (9K) was raised against the peptide sequence: CHTVGGRPSRKFRPR. The pUL37 tegument protein was detected with rabbit polyclonal antibody D1789 at a dilution of 1:2500, as described previously (Coller and Smith, 2008). Secondary antibodies conjugated to horseradish peroxidase were acquired from Jackson ImmunoResearch and used at following dilutions: 1:30,000 bovine anti-goat, 1:10,000 goat anti-mouse, 1:50,000 goat anti-rabbit, 1:5000 rabbit anti-chicken.

Cell Transfection and treatment with inhibitors. For figures 1, 2B, 1S, 2S panel B, and 3S, Vero cells were transfected with expression plasmids using polyethylenimine (PEI, Polysciences, catalog no. 23966) as follows: a confluent plate of Vero cells was split 1:5 into 6-well plate (VWR) containing sterile glass coverslips (22 x 22 mm, #1.5, VWR) and incubated with PEI-DNA mixture (to 200 ml of DMEM, 9 µl of PEI and 1-5 µg of DNA were added, mixed and incubated for 10 min at RT). Cells were imaged 16-28 h post transfection. In a subset of experiments, cells were treated with 10 µM nocodazole or 0.5 µM cytochalasin D for either 1 h (Fig. 2S panel B) or 4.5-5 h (Fig. 3S) before imaging. For figures 2A, 2S panel A, movie 1 and movie 2, Vero cells were transfected with Lipofectamine 2000 (Invitrogen) according to the manufacturer's protocol. Freshly seeded Vero cells (as above) were incubated with a DNA-Lipofectamine 2000 mixture (0.5-3 µg of DNA and 6 µl of Lipofectamine 2000 in 250 ml of DMEM per well) for 20-28 h before imaging. For co-immunoprecipitation experiments, subconfluent HEK293 cells were transfected with a DNA-Lipofectamine 2000 mixture (0.5-4 µg of DNA and 6 µl of Lipofectamine 2000 in 250 ml of DMEM per well) for 18-24 h before cell lysis. Transfection efficiency was monitored based on GFP fluorescence, and in all cases was above 30%.

Co-immunoprecipitation and Western Blot Analysis. HEK293 cells transiently expressing GFP and GFP-tagged VP1/2 mutants were treated with 10 µM nocodazole (VWR) for 1 h, washed once with cold

PBS supplemented with 0.1 mM phenylmethylsulfonyl fluoride, and lysed 18-24 h post-transfection in 500 µl/well of cold TAP lysis buffer (50 mM Tris-HCl pH 7.5, 50 mM KaCl, 2 mM $MgCl_2$, 0.1 mM EDTA, 5% glycerol, 1% NP-40) supplemented with 10 µM nocodazole, 1 mM dithiothreitol, 0.5 mM NaF, 0.1 mM Na_3VO_4, 0.1 mM phenylmethylsulfonyl fluoride (PMSF), and a protease inhibitor cocktail (P1860, Sigma) according to the manufacturer's protocol. A total of 2.5 µl of anti-GFP rabbit serum (Invitrogen) was bound to 100 µl of a Sepharose A/G bead slurry (CalBiochem) (washed two times with cold PBS and three times with cold TAP lysis buffer) for 2 h at 4°C. Beads were washed three times with cold TAP lysis buffer to remove unbound antibody. Approximately 800 µl of precleared (centrifuged at 14,000 x g for 10 min) lysate was incubated with a 15 µl aliquot of the antibody-bound beads overnight (12-14 h) at 4°C. The beads were washed four times with cold TAP lysis buffer supplemented with 2 µM nocodazole, 1 mM dithiothreitol, 0.5 mM NaF, 0.1 mM Na_3VO_4 and 0.1 mM PMSF and then resuspended in 60 µl (30 µl for Fig. 3B) of 4x final sample buffer (125 mM Tris-HCl pH 6.8, 20% glycerol, 2% SDS, 0.02% bromophenol blue) supplemented with 10% ß-mercaptoethanol. Samples were heated at 75°C for 20 min, divided into two equal parts (with the exception of Fig. 3B), separated on 7% and 10% sodium dodecyl sulfate-polyacrylamide gel or 4-20% precast Mini-PROTEAN TGX gels (Bio-Rad), and transferred to PVDF Hybond-P membranes (GE Healthcare). 30 µl of appropriate cell lysates were run in parallel with experimental samples as "input" control (6% of total input). The membrane was blocked with 5% dry nonfat milk in 1x TBST (0.1% Tween 20 in Tris-buffered saline) for 1.4 h at room temperature, then incubated with an appropriate dilution of primary antibody at 4°C overnight, followed by a horseradish peroxidase-conjugated goat anti-mouse antibody used at a 1:10,000 dilution (Jackson ImmunoResearch). Proteins of interest were visualized using a luminol-coumeric acid-H_2O_2 chemiluminescence solution, and exposed film was digitized with an Epson Perfection V500 photo scanner. Densitometry analysis was performed using ImageJ software and plotted in Excel. Basic ratio of density of co-immunoprecipitated protein over density of immunoprecipitated (eluted) protein was used to analyze the interaction of VP1/2 mutants with dynactin subunits. All antibodies were diluted in 1% dry nonfat milk in 1x TBST. Primary antibodies were used in this study as follows: 1:1,000 dilution of mouse monoclonal anti-GFP (B2, SantaCruz), anti-dynamitin/p50 (Abcam), anti-p150glued (BD Biosciences), anti-dynein intermediate chain (DIC 74.1, Chemicon), and anti-α-tubulin (DM1A, Abcam).

Sucrose density gradient sedimentation. HEK293 cells were transfected as described above. At least two confluent 10 cm dishes were transfected with Lipofectamine 2000 for each sample (as described above). Cells were collected 48 hpt by scraping and washed twice with cold PBS (supplemented with 0.1 mM PMSF). Cell pellets were lysed for 2 hours at 4°C in 600 µl of modified TAP buffer (50 mM Tris-HCl pH 7.5, 50 mM KaCl, 2 mM $MgCl_2$, 0.1 mM EDTA, 5% Sucrose, 1% NP-40) supplemented with 10 µM nocodazole, 1 mM dithiothreitol, 0.5 mM NaF, 0.1 mM Na_3VO_4, 0.1 mM PMSF, and 1:100 protease inhibitor cocktail (P1860, Sigma). Half way through the incubation, cell lysates were pushed 10 times through 27½ G needle. Cell debris was cleared by centrifugation at 18,000 x g for 20 min at 4°C. 500 µl of cleared lysate was then transferred to a 10 to 40% continuous sucrose gradient made in modified TAP buffer with a Gradient Master (BioComp Instruments). After a 19 h centrifugation at 260,000 x g at 4°C in a SW41 rotor, twelve ≈ 0.9 ml fractions were collected using a Gradient Fractionator (BioComp Instruments). 25 µl of each fraction were separated on 4-20% precast Mini-PROTEAN TGX gels alongside samples of 2% of total cell lysate and 3% of resuspended cell pellet. Protein was transferred to a PVDF Immobilon-FL membrane (Invitrogen) and probed by Western blot as described above.

Live-cell fluorescence microscopy and image analysis. For figures 1, 2A, 4, 5, 6, 1S panel A, 2S, and movie 1, images were acquired with an inverted wide-field Nikon Eclipse TE2000-E fluorescence microscope fitted with a 60×1.4 numerical aperture (NA) objective and a Photometrics CoolSnap HQ2 camera. For figures 2B, 3S, and 1S panel B images were acquired with a Cascade 650 charged-coupled camera (Photometrics, Roper Scientific). All microscopes were housed in a 37°C environmental box (In Vivo Scientific) and infected or transfected cells were imaged in VALAB (Vaseline, lanolin, and beeswax) sealed chambers as previously described (Smith et al., 2001). Image acquisition and processing was done with MetaMorph (Molecular Devices, Downington, PA) and ImageJ software. Still images were taken in the following order: differential interference contrast (DIC) followed by 100 ms GFP. For figures 2B and 3S, mitochondria were stained with Mito-tracker Red CMXRos (1:10,000; Invitrogen) according to the manufacture's protocol, and a 30 ms RFP exposure was included between the DIC and GFP captures.

Animal studies. Animals (CD-1 mice and Long-Evans rats, males, Charles River) were maintained under 12 h light: 12 h dark conditions throughout with food and water continuously available. All procedures conformed to NIH guidelines for work with laboratory animals and were approved by the Institutional Animal Care and Use Committee of the University of Nebraska, Lincoln.

Intranasal infection of CD-1 mice was performed as previously described (Bohannon et al., 2012). Briefly, each CD-1 mouse (8-10 weeks old,) received 5 µl of PRV (6-8.5 x 10^5) into each nostril while anesthetized by isofluorane (2.5-5.0%) inhalation. Behavior was continuously video monitored and images were captured every 10 min. Time to death after inoculation was determined from recorded images and rounded to the nearest hour. P-values were determined by a Tukey's multiple comparison test.

Intraocular injections of male Long Evans rats were previously described (Lee et al., 2009). Briefly, animals (at least 14 weeks of age) were anesthetized via isoflurane inhalation anesthetic (2.5–5%), and received a unilateral anterior chamber injection of 2 µl of either PRV-GS2111 (1.6 x 10^8 pfu/ml) or PRV-GS4079 (1.7 X 10^8 pfu/ml) over a 1 min interval using a Nanoject II nanoinjector fitted with a glass micropipette (Drummond Scientific Co, Broomall, PA). A fresh stock of virus was thawed for each injection. Animals were maintained in a biosafety level 2 facility for up to 5 days post-inoculation.

Brain tissue was prepared as described previously (Lee et al., 2009). Briefly, after post-injection intervals ranging from 1–5 days, animals were deeply anesthetized with sodium pentobarbital (80 mg/kg, i.p.), and perfused transcardially with 0.9% saline followed by freshly prepared fixative consisting of 4% paraformaldehyde in phosphate buffer (0.1 M), pH 7.3. Of 18 animals infected with PRV-GS4079, three were sacrificed at 24 h.p.i., eight at 36 h.p.i., three at 48 h.p.i., four between 68 and 73 h.p.i., and one succumbed to infection at 70 h.p.i.). Animals infected with the PRV-GS2111 were sacrificed between 70 and 120 h.p.i as follows: 3 at 70-72 h.p.i., 7 at 90-97 h.p.i., and 5 at 119-120 h.p.i. Brains and SCGs were removed, stored in the same fixative containing 30% sucrose at 4°C overnight, and sectioned at 40 µm in the coronal plane on a sliding microtome equipped with a freezing stage (Physitemp Instruments Inc., Clifton, NJ). Sections were collected in phosphate buffer, mounted on subbed slides, blotted to remove excess buffer, and coverslipped with Vectashield mounting medium (Vector Laboratories, Burlingame, CA). Coverslips were sealed with fingernail polish to prevent dehydration, and slides were stored in the dark at 4°C. Slides were examined using a Leica (Nussloch, Germany) DMRA light microscope equipped with epifluorescence.

Supplemental References

Abramoff, M.D., Magelhaes, P.J., and Ram, S.J. (2004). Image Processing with ImageJ. Biophotonics International *11*, 36-42.

Antinone, S.E., and Smith, G.A. (2006). Two modes of herpesvirus trafficking in neurons: membrane acquisition directs motion. J Virol *80*, 11235-11240.

Bear, J.E., Loureiro, J.J., Libova, I., Fassler, R., Wehland, J., and Gertler, F.B. (2000). Negative regulation of fibroblast motility by Ena/VASP proteins. Cell *101*, 717-728.

Bohannon, K.P., Sollars, P.J., Pickard, G.E., and Smith, G.A. (2012). Fusion of a fluorescent protein to the pUL25 minor capsid protein of pseudorabies virus allows live-cell capsid imaging with negligible impact on infection. J Gen Virol *93*, 124-129.

Bubeck, P., Pistor, S., Wehland, J., and Jockusch, B.M. (1997). Ligand recruitment by vinculin domains in transfected cells. J Cell Sci *110 (Pt 12)*, 1361-1371.

Coller, K.E., Lee, J.I., Ueda, A., and Smith, G.A. (2007). The capsid and tegument of the alphaherpesviruses are linked by an interaction between the UL25 and VP1/2 proteins. J Virol *81*, 11790-11797.

Coller, K.E., and Smith, G.A. (2008). Two viral kinases are required for sustained long distance axon transport of a neuroinvasive herpesvirus. Traffic *9*, 1458-1470.

Hoogenraad, C.C., Wulf, P., Schiefermeier, N., Stepanova, T., Galjart, N., Small, J.V., Grosveld, F., de Zeeuw, C.I., and Akhmanova, A. (2003). Bicaudal D induces selective dynein-mediated microtubule minus end-directed transport. EMBO J *22*, 6004-6015.

Lee, J.I., Luxton, G.W., and Smith, G.A. (2006). Identification of an essential domain in the herpesvirus VP1/2 tegument protein: the carboxy terminus directs incorporation into capsid assemblons. J Virol *80*, 12086-12094.

Lee, J.I., Sollars, P.J., Baver, S.B., Pickard, G.E., Leelawong, M., and Smith, G.A. (2009). A herpesvirus encoded deubiquitinase is a novel neuroinvasive determinant. PLoS Pathog *5*, e1000387.

Leelawong, M., Lee, J.I., and Smith, G.A. (2012). Nuclear egress of pseudorabies virus capsids is enhanced by a subspecies of the large tegument protein that is lost upon cytoplasmic maturation. J Virol *86*, 6303-6314.

Luxton, G.W., Haverlock, S., Coller, K.E., Antinone, S.E., Pincetic, A., and Smith, G.A. (2005). Targeting of herpesvirus capsid transport in axons is coupled to association with specific sets of tegument proteins. Proc Natl Acad Sci U S A *102*, 5832-5837.

Smith, B.N., Banfield, B.W., Smeraski, C.A., Wilcox, C.L., Dudek, F.E., Enquist, L.W., and Pickard, G.E. (2000). Pseudorabies virus expressing enhanced green fluorescent protein: A tool for in vitro electrophysiological analysis of transsynaptically labeled neurons in identified central nervous system circuits. Proc Natl Acad Sci U S A *97*, 9264-9269.

Smith, C.L. (1998). Culturing nerve cells, G. Banker, and K. Goslin, eds. (Cambridge, MA, MIT Press).

Smith, G.A., and Enquist, L.W. (1999). Construction and transposon mutagenesis in Escherichia coli of a full-length infectious clone of pseudorabies virus, an alphaherpesvirus. J Virol *73*, 6405-6414.

Smith, G.A., Gross, S.P., and Enquist, L.W. (2001). Herpesviruses use bidirectional fast-axonal transport to spread in sensory neurons. Proc Natl Acad Sci U S A *98*, 3466-3470.

Smith, G.A., Pomeranz, L., Gross, S.P., and Enquist, L.W. (2004). Local modulation of plus-end transport targets herpesvirus entry and egress in sensory axons. Proc Natl Acad Sci U S A *101*, 16034-16039.

Szpara, M.L., Tafuri, Y.R., Parsons, L., Shamim, S.R., Verstrepen, K.J., Legendre, M., and Enquist, L.W. (2011). A wide extent of inter-strain diversity in virulent and vaccine strains of alphaherpesviruses. PLoS Pathog *7*, e1002282.

Tirabassi, R.S., and Enquist, L.W. (1998). Role of envelope protein gE endocytosis in the pseudorabies virus life cycle. J Virol *72*, 4571-4579.

Tischer, B.K., von Einem, J., Kaufer, B., and Osterrieder, N. (2006). Two-step red-mediated recombination for versatile high-efficiency markerless DNA manipulation in Escherichia coli. Biotechniques *40*, 191-197.